Received: 22 February 2022 | Revised: 28 March 2022 | Accepted: 8 April 2022

DOI: 10.1002/eom2.12212

RESEARCH ARTICLE

EcoMat FUNCTIONAL MATERIALS FOR GREEN ENERGY AND ENVIRONMENT WILEY

Ultra-fast, low-cost, and green regeneration of graphite anode using flash joule heating method

Shu Dong | Yali Song | Ke Ye | Jun Yan | Guiling Wang | Kai Zhu | Dianxue Cao

College of Material Science and Chemical Engineering, Harbin Engineering University, Harbin, China

Correspondence
Kai Zhu and Dianxue Cao, College of Material Science and Chemical Engineering, Harbin Engineering University, Harbin 150001, China.
Email: kzhu@hrbeu.edu.cn and caodianxue@hrbeu.edu.cn

Funding information
China Postdoctoral Science Foundation, Grant/Award Numbers: 2018M630340, 2019T120254; National Natural Science Foundation of China, Grant/Award Numbers: 51702063, 51672056; Natural Science Foundation of Heilongjiang Province, Grant/Award Number: LC2018004

Abstract

Graphite is the state-of-the-art anode material for most commercial lithium-ion batteries. Currently, graphite in the spent batteries is generally directly burned, which caused not only CO_2 emission but also a waste of precious carbon resources. In this study, we regenerate graphite in lithium-ion batteries at the end of life with excellent electrochemical properties using the fast, efficient, and green Flash Joule Heating method (FJH). Through our own developed equipment, under constant pressure and air atmosphere, graphite is rapidly regenerated in 0.1 s without pollutants emission. We perform a detailed analysis of graphite material before and after recovery by multiple means of characterization and find that the regenerated graphite displays electrochemical properties nearly the same as new graphite. FJH provides a large current for defect repair and crystal structure reconstruction in graphite, as well as allowing the SEI coating to be removed during ultra-fast annealing. The electric field guide the conductive agent and binder pyrolysis products to form conductive sheet graphene and curly graphene covering the graphite surface, making the recycled graphite even better than new commercial graphite in terms of electrical conductivity. Regenerated graphite has excellent multiplier performance and cycle performance (350 mAh g^{-1} at 1 C with a capacity retention of 99% after 500 cycles). At cost, we get recycled graphite that displays the same performance as new graphite, costing just 77 CNY per ton. This FJH method is not only universal for the regeneration of spent graphite generated by various devices but also enables multiple use-failure-regeneration steps of graphite, showing great potential for commercial applications.

KEYWORDS

flash joule heating method, graphite regenerate, lithium-ion battery, low-cost

1 | INTRODUCTION

Lithium-ion batteries (LIBs) have been widely used in consumer electronics and become the leading power source for electric vehicles (EVs) due to their long lifespan and high energy density.[1,2] Battery energy storage reached 5 GW in 2020, growing more than any historical period, and is expected to reach 600 GW by 2030, among which the requirement of LIBs still keeps rapid growth, due to the popularization of EVs and updated electronic products.[3] Considering the limited service life of the LIBs, a large amount of spent LIBs will be disposed of in the next 5–10 years. Therefore, the high-efficiency and environmental recycling of LIBs, especially the value-add electrode materials, becomes a crucial issue.[4,5]

Graphite is unbeaten the most suitable anode material and almost denominates the whole anode market at present, due to its merits of high electric conductivity, low working voltage, and suitable theoretical capacity.[6,7] During the discharging process, Li-ion intercalates into the layered graphite to form Li_xC_6 ($0 \leq x \leq 1$) compounds. Meanwhile, electrolyte would decompose and a solid electrolyte interface is generated on the surface of the graphite, serving as a passive protective layer.[8] Usually, 1 kg graphite could meet the requirement of 1 kWh batteries.[9] Thus, the spent graphite anode caused by LIBs is expected to reach over 180 000 tonnes per year in the future.[10] Seeking the low-cost regenerate techniques of consumables can promote the virtuous cycle development of the whole industry. However, several issues need to be solved for the graphite electrode materials recycling: (i) difficult removal of the inert binder and perishable SEI from the spent graphite; (ii) electrochemical performance recovery of exhausted graphite electrode; and (iii) rapid and low-cost recycling technology without tedious approach and acid/alkali treatment. It is still a challenge to develop an effective technique to achieve large-scale spent graphite recycling.[11,12]

Recently, a novel flash joule heating (FJH) technique is employed to convert the precursors into bulk quantities of nanomaterials, such as flash transition metal dichalcogenides, fluorinated nanodiamond, and graphene, via a direct current discharge from large capacitors.[13,14] The FJH uses the characteristics of the capacitor instantaneous discharge and the change of resistance before and after the material reaction to reach more than 400 A of current at a lower voltage and releases the corresponding energy to produce a flash (combustion) reaction. During the preparation process, a high temperature of more than 3000 K can be achieved in a short time of 0.01 S. The FJH is considered a promising high-temperature materials synthesis technique due to avoiding tedious heating steps.[15,16]

Herein, we realized bulk quantities of spent graphite recycling in a short time through the modified FJH technique. The high-temperature environment (>3000 K)[13] promises the effective removal of binder (thermo-decomposed temperature <600 K), the component of SEI, such as LiF (volatilize temperature <1500 K) and Li_2CO_3 (boiling point <1700 K), and lithium embedded in graphite layer (boiling point <1600 K).[17] Meanwhile, graphite layered structure is restored and electrochemical performance is recovered. Recycled graphite presents a capacity of 343 mAh g^{-1} at 1 C with a capacity retention of 99% after 500 cycles. This work provides an innovative FJH approach to realize the concurrent reuse of spent graphite anode and demonstrate the effect of high temperature on electrochemical performance recovery of the electrode.

2 | RESULTS AND DISCUSSION

The details of the FJH setup are shown in Figure 1. The spent graphite electrode materials are filled in the quartz tube reaction vessel, which is connected with a series of the independently-controlled capacitor of 5.6 mF by graphite rods contact media. The detailed circuit diagram and the selection of components specifications are detailed in Figures S1, S2, and Table S1. The theoretical reaction energy can be adjusted by using different amounts of capacitors in the same reaction time and voltage according to the followed Equation (1):

$$E = \left(V_1^2 - V_2^2\right) \times \frac{C}{2} \times M \quad (1)$$

E is the energy consumed, V_1 and V_2 are the capacitor initial voltage and post-reaction voltage, C is the capacity of the capacitor, and M is the quality of reactive materials.[9] In this work, three types of flashed graphite (F-RG) are obtained by using 2, 5, and 10 capacitors to release energy at 200 V voltage, corresponding to the reaction energy of 22.4, 56, 112, respectively. The strong flash is observed due to the occurrence of carbonation of binder, volatilization of electrolyte, gasification of lithium metal, and decomposition of SEI components in less than 1 s. In contrast, such a flash phenomenon does not happen for commercial graphite materials during the FJH process (Video S1, Data S1).

Figure 2A,D the SEM images of spent graphite and the F-RG after energy hitting using 112 kJ g^{-1}, respectively. The spent graphite electrode presents 8 μm of particle size with strong agglomeration caused by the presence of a binder. The wrapped binder can be seen in

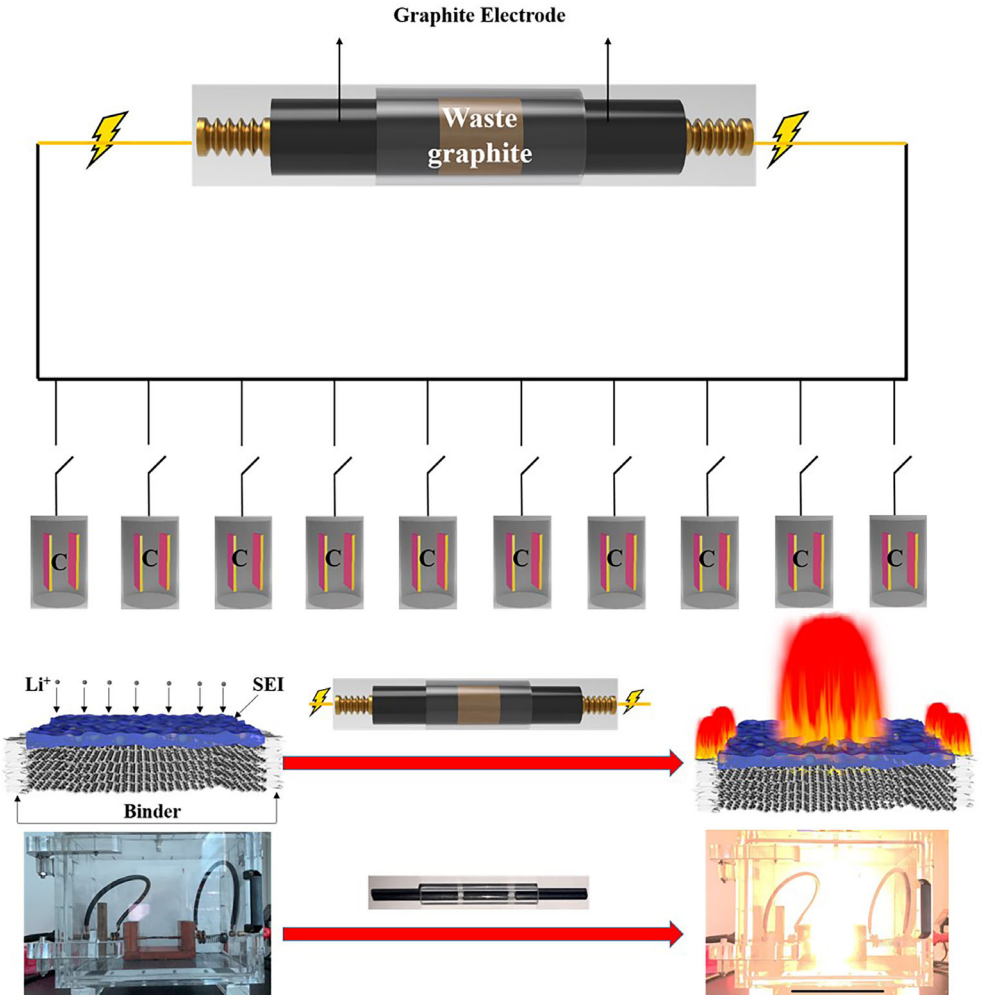

FIGURE 1 Schematic illustration of FJH discharge equipment and regeneration of spent graphite electrode materials

Figure S3. After the FJH process, the F-RG displays a slightly decreased size without cracking, suggesting the successful removal of the binder. Meanwhile, some sheet-like graphite is also found because the FJH process is in favor of exfoliating bulk materials into two-dimensional materials.[15] To further investigate the surface condition of the spent graphite and F-RG, the TEM testing was carried out. The spent graphite shows a particle size of 2–3 μm with agglomeration and a thick SEI layer is observed on its surface. (Figure 2B,C). In contrast, the F-RG displays a sheet-like morphology, which is exfoliated from the graphite during the FJH process. Some small particles are attached to the sheet, which may be ascribed to the carbonization of the binder. It should be noticed that the graphite dispersion becomes better with increasing electric shock energy (Figure S4, and Figure 2D–F), demonstrating the high electric shock energy in favor of carbonization of binder and the gasification of other components. Meanwhile, the HRTEM image (Figure 2F) shows a smooth surface of F-RG, suggesting the SEI film completely disappeared. The EDS mapping was also performed to confirm the SEI film on the graphite before and after the FJH process. As shown in Figure 2G,H, the C element is dispersed uniformly in the material and the O, F, and P elements gather around the surface of the material, which evidences the thick SEI on the spent graphite. On the contrary, the O, F, and P elements on the F-RG are unobservable, further indicating the successful removal of SEI.

Figure 3A displays the XRD of the spent graphite and F-RG under different reaction energies. All the materials show the peaks belonging to the typical 2H graphite phase.[18] With increasing reaction energy, the diffraction peak representing the 002 plane gradually shifts to a small angle, indicating the disappearance of the SEI on the graphite surface at high temperatures. The interlayer spacing d (nm) is calculated based on the Bragg law ($2d\sin\theta = n\lambda$, in which θ (°) is the diffraction angle, λ (nm) is the wavelength, n is the reflective series). The F-RG hit by 112 kJ g^{-1} presents a larger interlayer spacing of 3.389 Å compared with the spent graphite (3.363 Å), which favors regenerating graphite more adaptable to volume expansion during lithiation.[19] Meanwhile, the Raman spectra were carried out to confirm the effect of

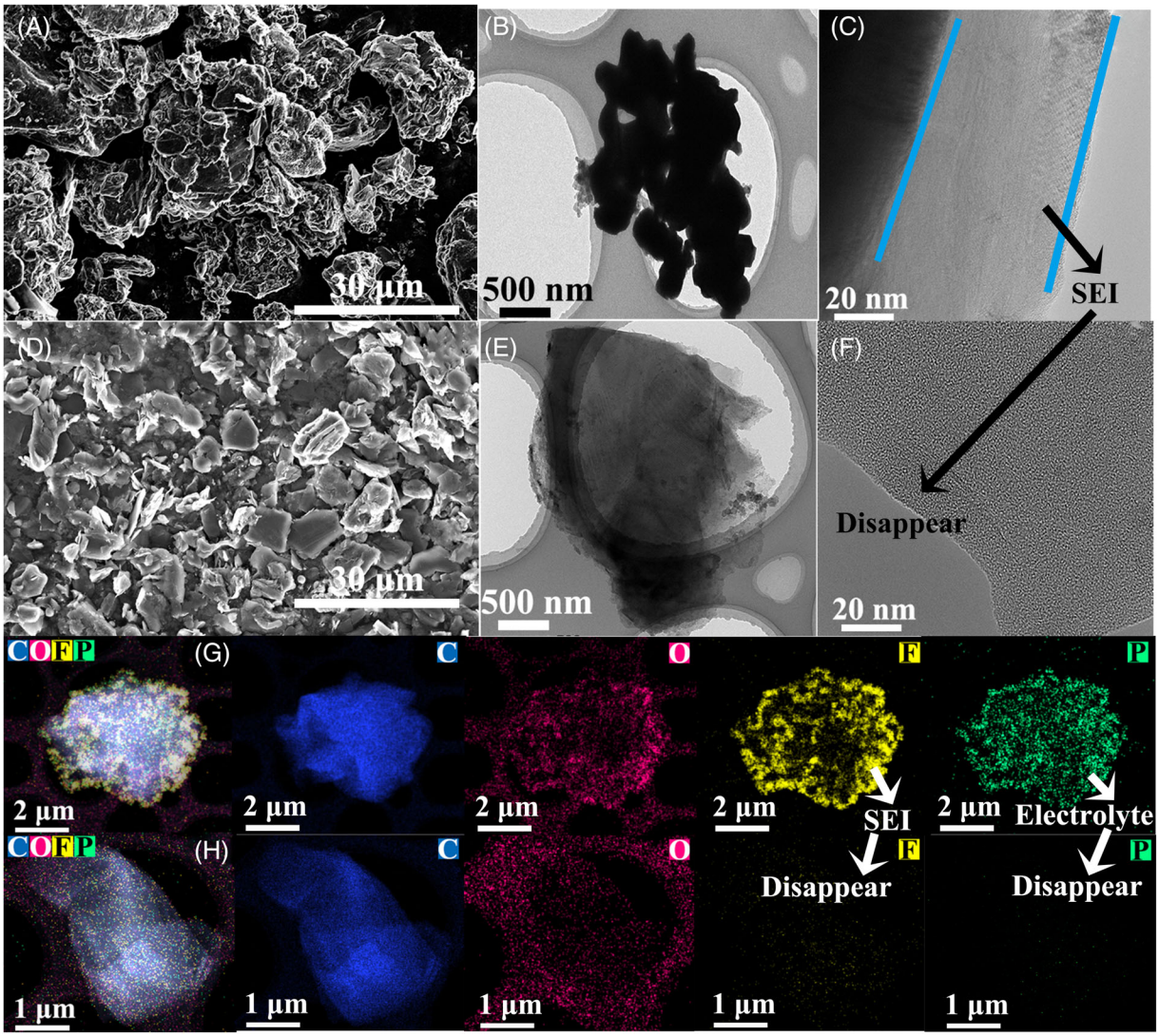

FIGURE 2 SEM and TEM images of (A–C) spent graphite, and (D–F) F-RG. (G) The Mapping of C, O, F, P in spent graphite, and (H) in F-RG

the FJH process on the graphite reconstruction. Spent graphite and F-RG under different reaction energy display peaks at around 1340, 1580, 2700, and 3225 cm^{-1}, corresponding to the typical D, G, 2D, and 2G bands, respectively.[20] Usually, the D band and G band are ascribed to the breathing mode and stretching mode of sp^2 hybridized carbon, respectively. The intensity ratio of the D band to the G band (I_d/I_g) can be calculated to represent the degree of the graphitization.[15] The spent graphite shows an I_d/I_g of 0.64, suggesting a large disorder of carbon due to the repeated Li-ion (de)intercalation process. With increasing the energy of the FJH process, the I_d/I_g is decreased. When the energy is 112 kJ g^{-1}, I_d/I_g of the F-RG is 0.103, demonstrating the FJH process could reconstruct the carbon structure and enhance the degree of the graphitization. In addition, infrared spectroscopy tests are performed to verify the removal of the impurity. The spent graphite presents several peaks at 1766, 1632, 1195, 1080, and 1767 cm^{-1} in FTIR spectra (Figure 3C), which can be attributed to the stretch vibration of C=O, C=C (aromatic nucleus), C-O (alkyl oxygen) from the commercial anode binder.[21–24] The observed peaks at 877 cm^{-1} are attributed to the CO_3^{2-} content in the SEI.[25] However, in the F-RG, expect the telescopic vibration absorption peak of C—C at 1049 cm^{-1} symbolizing the conductivity agent, other abovementioned peaks disappear or extremely decrease, confirming the removal of the impurity.[26] The disappearance of F, P, and Li peaks and weakened O peaks in the F-RG XPS (Figure 3D) is ascribed to the removal of SEI film during the FJH process. Figure S5 presents the element content in the spent graphite and F-RG respectively according to the XPS analysis. The peaks belonging to Li, P, and F disappear in the F-RG. The C content rose

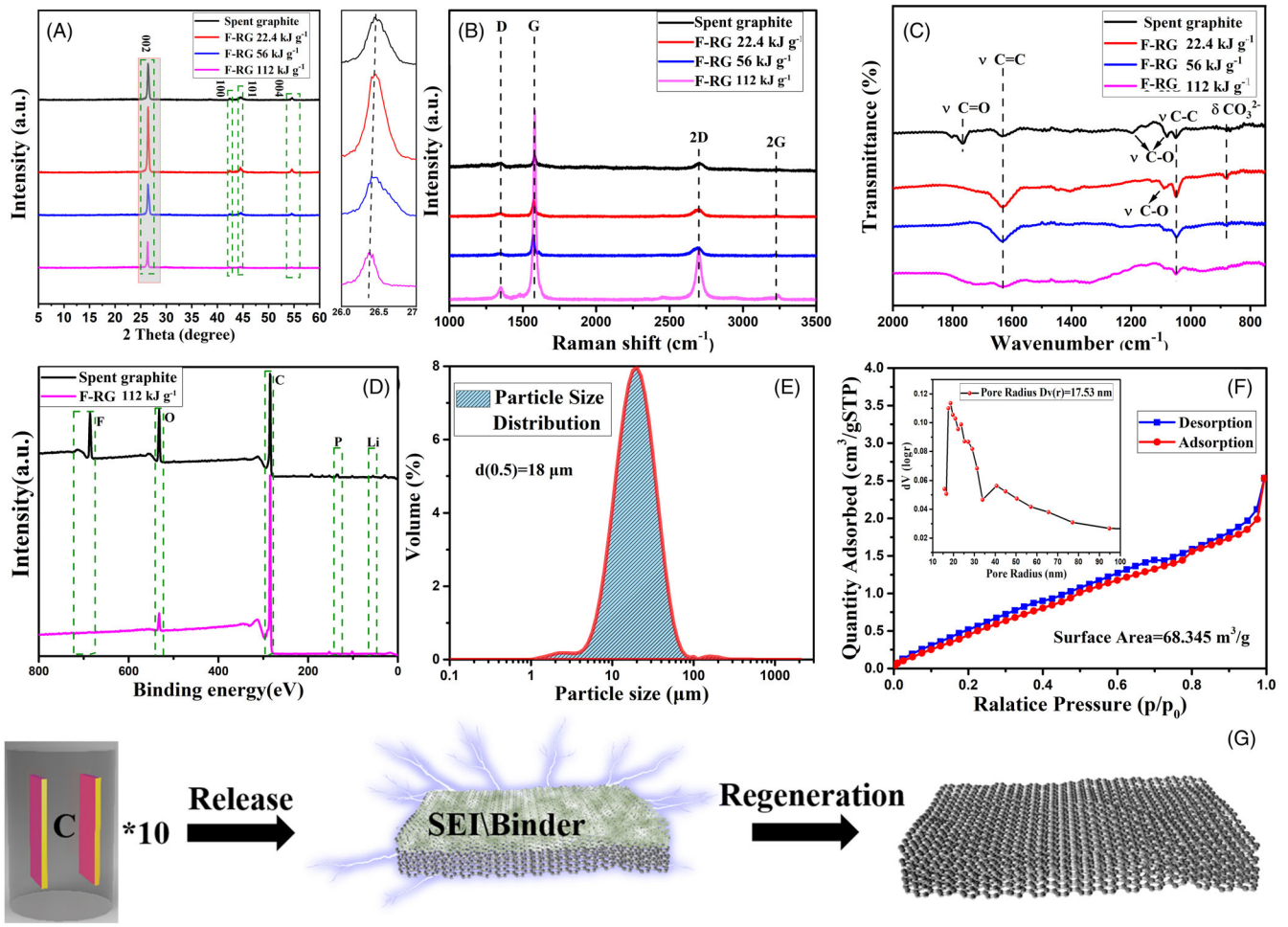

FIGURE 3 (A) XRD patterns, (B) Raman spectra, and (C) FTIR spectrum of spent graphite and F-RG with different energies. (D) XPS spectra of spent graphite and F-RG with the energy of 112 kJ g^{-1}. (E) Particle size distribution of F-RG with the energy of 112 kJ g^{-1}. (F) BET of F-RG with the energy of 112 kJ g^{-1}. (G) Schematic representation of the graphite regeneration

from 62.6% (spent graphite) to 94.21% (F-RG) and the content of Li, F, P, O decreased greatly, demonstrating the removal of the SEI layer and binder. Moreover, the ICP and TG results also demonstrate the disappearance of the residues. The F-RG still retained 98% of its initial weight after the heat treatment at 1200 K. indicating the significantly reduced volatile components in the graphite during the FJH process. In contrast, the mass retention of the spent graphite is only 60%. This result is in perfect agreement with the XPS results, indicating that the Joule heat generated in the FJH process is higher than 1200 K, thus a large amount of noncarbon ingredients is removed (Figures S6, S7). The spent graphite has an average particle diameter of 28 μm (Figure S8). In contrast, the average particle diameter of F-RG is significantly reduced to 18 μm due to the removal of the binder. (Figure 3E) Meanwhile, the F-RG shows a large surface area of 68.345 m^3 g^{-1} than spent graphite (1.6907 m^3 g^{-1}) as shown in Figure 3F and Figure S9. The above results demonstrate that the binder, SEI film, lithium-ion interlayer compound, and residual electrolyte in spent graphite would be vaporized and carbonized at high temperature after the FJH method as illustrated in Figure 3G.

We assembled the F-RG hitting by 112 kJ g^{-1} into the battery as the new anode. The cyclic voltammetry (CV) was carried out to investigate the electrochemical performance of the F-RG as shown in Figure 4A. F-RG presents reduction peaks located at ~1.5 V and ~ 0.6 V in the first cycle due to the new SEI generation.[27] In the following cycles, the CV curves keep well, suggesting the reversible Li-ion intercalation and extraction process. Meanwhile, the CV curves of F-RG under various scan rates from 0.2 to 5 mV s^{-1} do not show an obvious polarization in Figure S10, demonstrating the fast Li-ion storage ability. F-RG display obvious Li-ion intercalation plateaus with a discharge capacity of 398 mAh g^{-1} and a charge capacity of 385 mAh g^{-1} in the first cycle,

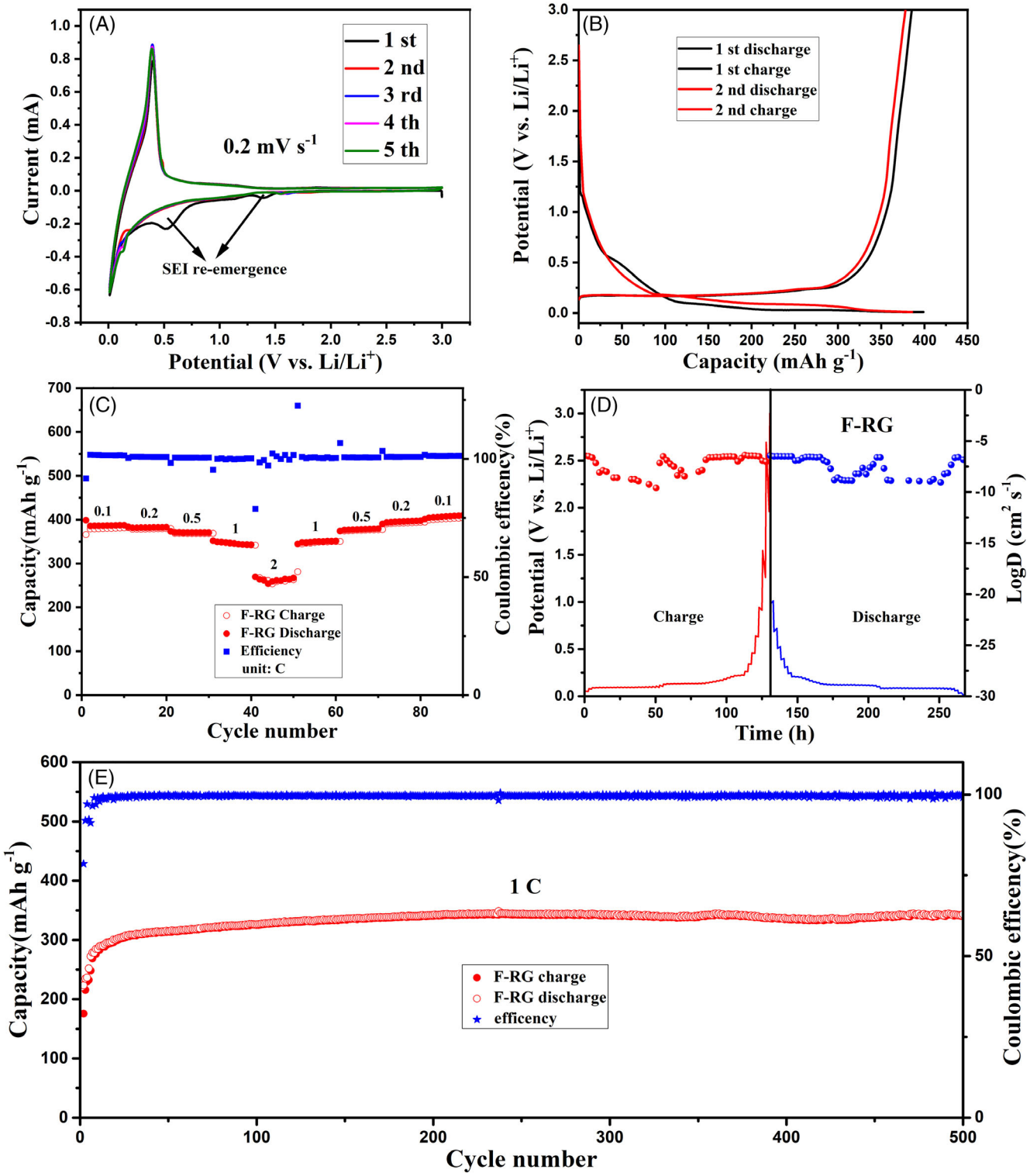

FIGURE 4 Electrochemical performances of the regenerate anode. (A) First 5 cycles of CV curves by F-RG. (B) First 3 cycles of GCD curves by F-RG at the current density of 0.1C. (C) Rate performance at current densities of 0.1 to 2 C. (D) The GITT curves of F-RG. (E) Cycle performance and Coulombic efficiency at the current density of 1 C of F-RG

corresponding to an Initial Coulombic Efficiency (ICE) of 91.7%. The irreversible capacity can be attributed to the SEI generation. In the second cycle, the plateau at 0.5 V disappears, and the Coulombic Efficiency increase to 98.1%. F-RG also show a capacity of 387, 381, 371, 350, 277 mAh g^{-1} at 0.1, 0.2. 0.5, 1, 2 C, respectively, demonstrating a good rate ability. When the current density step-by-step return to 0.1 C, a capacity of 370 mAh g^{-1}

can be obtained (Figure 4B). In contrast, the spent graphite shows the specific capacity of 271, 265, 250, 220, 150 mAh g^{-1} at 0.1, 0.2, 0.5, 1, 2 C, respectively, suggesting the FJH process could effectively enhance the electrochemical performance of spent graphite (Figure S11). Figure S12 displays EIS tests on spent graphite and F-RG half cells. F-RG displays a charge transfer resistance (R_{ct}) of 40 Ω lower than that of spent graphite (315 Ω), resulting in the enhanced rate performance. We additionally tested the EIS of half-cells assembled by regenerated graphite and new commercial graphite in the initial state. The R_{ct} of F-RG with the added conductive agent is much smaller than that of commercial graphite with the added conductive agent (180 Ω), demonstrating the superior conductivity of the F-RG. In addition, the diffusion coefficient of the Li ions in the F-RG was calculated by the galvanostatic intermittent titration technique (GITT). The F-RG shows diffusion coefficients in arrange from the 10^{-6} to 10^{-9} cm^2 s^{-1}, which is comparable with previously reported graphite materials.[28] As shown in Figure 4E, after the activation process (the initial 20 cycles), F-RG exhibits a stable cycling performance with a capacity retention of 99% after 500 cycles, corresponding to a capacity decay of 0.02% per cycle, which is much better than the spent graphite (capacity retention of 95%, Figure S13).

The enhanced cycling performance is ascribed to the reconstructed graphite phase of F-RG during the FJH process. Graphite is a kind of material with a high degree of anisotropy. For graphite, the mobility of electrons is ballistic (about 2.26×10^4 S cm^{-1}) in the basal plane, but rather a poor perpendicular to them (5.9 S cm^{-1}). According to the reports of James M. Tour,[14,15] the current follows the path of lowest resistance, thus providing maximum heat to the conductive region. The material in and around the conductive route will be annealed and graphitized extensively, gradually improving conductivity until all imperfections have been eradicated. Recovered graphite generates significant Joule heat during the FJH process as the current flows along the lamellar plane of the graphite and the conductive agent-graphite contact surface. As a result, the low-volatile-point components in SEI are removed, while the surrounding conductive agent (SP) supplies highly mobile amorphous carbon to facilitate the formation of the graphene lamellae morphology. Although the pyrolysis carbon products of SP and binder in the waste graphite cannot be completely removed, surprisingly, the presence of these substances has a favorable effect on the structural recovery and electrical conductivity of the recovered graphite. Benefit from the conductive agent on the surface and the pyrolysis products of the binder, carbon atoms reorganize and carbon radicals fill the pores at high temperatures to form a near-perfect carbon lattice consistent with graphene, repairing the defects of the graphite structure after charging and discharging cycles. The surrounding amorphous carbon has no rigid predefined structure and, during the FJH process, undergoes rapid graphitization, forming a graphene-like layer on the graphite surface. Furthermore, the SP centroid particles are subjected to slow thermal defect annealing to generate folded graphene bonded to the graphite surface, which boosts the nascent graphite's electronic conductivity.

The lithium-ion full cell is assembled using the $LiFePO_4$ cathode and F-RG anode to confirm the potential application of F-RG. Figure S14 displays the CV curve of the F-RG||$LiFePO_4$ full cell. The typical oxidation and reduction peaks are located at 3.4 and 3.1 V, respectively, corresponding to the reversible lithium-ion intercalation and extraction process. The full cell delivers a reversible capacity of 120 mAh g^{-1} (based on the mass of cathode). After the activation process (20 cycles), the full cell shows good cycling stability with the capacity retention of 90% after 100 cycles, demonstrating the promising application of F-RG.

To verify the generality of the FJH method for the regeneration of the graphite anode in different devices. We regenerated the spent graphite from smartphone batteries by the same method. The XRD results (Figure S15) show that the spent anode derived from spent smartphone batteries contains graphite as well as a small amount of graphene, in addition to the SEI component deposited during charge–discharge cycles. After the FJH process, the anode impurities are greatly reduced, and the graphite layer spacing variations are similar to those seen in power batteries. FJH can not only remove other compounds deposited on graphite's surface, but it can also restore the graphite's crystal structure. After the cycle test, we dismantled the F-RG-based half-cell and obtained new spent graphite. Following the secondary FJH treatment, the 2F-RG was achieved. Figure S16 exhibits the performance of the negative electrode. After secondary recovery, the graphite electrode still recovered to its original performance, even accompanied by the increase of capacity at large current, which may be caused by the expansion of graphite layers. As a result, when combined with further graphite grading, the FJH process could realize several graphite anode regenerates.

We also put the FJH approach to the test in terms of recovering $LiFePO_4$ cathode from failed vehicular batteries (Figure S17). The results demonstrate that, while this approach improves the performance of $LiFePO_4$, it is still not up to commercial standards, possibly due to the lithium atoms lost during the battery cycle. Its lattice is heavily distorted, and the elemental content differs from the initial stoichiometric ratio, making it difficult to return to the original structure even at high temperatures. However, in circumstances with minimal capacity requirements, the

used cathode treated by FJH could be used as a cathode material. The regenerated anode, on the other hand, can meet commercial standards. As a result, the focus of this research is on anode recycling.

The final mass of F-RG can reach 60 mg while using 100 mg spent graphite. At a 60% yield, we cost only 77 CNY per ton of spent graphite (for 0.8 CNY per kWh, calculated with the industrial electricity charge in Harbin). This method does not involve a strong corrosive solvent or high-temperature reaction furnace. Furthermore, the product can be used directly without other additional treatment. Taken together, the F-RG achieves almost the same performance while being obtained at much lower than the cost of new graphite.[29] The results of small-scale laboratory testing were used to create the experiment described in this study. Industrial recycling involves complex technical routes, including shredding, electrolyte extraction, leaching, and precipitation.[30,31] FJH scheme can be combined with other sequence stages and only added to the manufacturing line as a step in the graphite processing process. As a result, we only take into account the cost of the FJH step.

We list comparison to other similar recent work which was shown in Table S2.[32–38] Compared with other processes, the graphite anode recovered by our method shows higher ICE, almost full recovery of capacity, very low cost, and short time consumption. This method is a cost-effective reported method for anode regeneration. However, the accuracy of this simple method is limited, and subsequent equipment improvement sessions need to be coupled with pressure sensors as well as machine learning to achieve high throughput and high accuracy responses. Some groups have already explored and made foresight in this area.[39] We will also aim to facilitate its application in practical production by coordinating complex variables during the FJH processes. The application of the methods described here is by far not limited to graphite regenerating in LIBs but can be expected to be successfully transferred to regeneration or carbonization of carbon materials in other types of spent batteries.

3 | CONCLUSIONS

In summary, we restore the electrochemical performance of spent graphite via a low-cost and rapid FJH method. The ultra-high temperature produced by the FJH method evaporates the inserted lithium, SEI film composition, and binder on the spent graphite, leading to a graphite structure reconstruction. When serving as anode materials for the lithium-ion batteries, The F-RG presents a high specific capacity of 343 mAh g^{-1} and excellent cycle stability at 1 C. Meanwhile, it could also be an available anode in the lithium-ion full cell with $LiFePO_4$ cathode. This work highlights a promising FJH method to recycle spent graphite anode and reconstruct the graphite structure, which would inspire the synthesis of carbon-based materials and promote graphite recycling.

4 | EXPERIMENTAL SECTION/METHODS

4.1 | Synthesis of F-RG

The spent LIBs are samples that failed to meet the standards of electric vehicles battery after cycle tests, provided by Harbin Guangyu Power Supply Co., Ltd. All spent battery requires a deep discharge before disassembly. The spent graphite powders were removed from the copper foil by placing the anode sheet carried out from the spent battery into 50 ml of deionized water (DI) and sonicated for 1 min, and was dried in the 80°C ovens for 12 h; 100 mg of spent graphite was added to the reaction vessel, the graphite electrodes were inserted on both ends afterward. After charging several parallel capacitors (2, 5, and 10) to 200 V, the energy was instantly released on the sample. Meanwhile, the phenomenon of "Flash" can be observed. The final product (F-RG) was collected as the anode for new LIBs. For the regeneration of spent $LiFePO_4$, the cathode is treated and dismantled in the same method. The spent graphite separated from the smartphone battery was treated by the same process.

4.2 | Material characterization

Transmission electron microscope (TEM) and scanning electron microscope (SEM) morphologies of F-RG were recorded from JEOL JEM-2100 and JEOL JSM7500F, respectively. The Brunauer–Emmett–Teller surface area was performed using Micro TriStar II Plus 2.02. Analyses of the crystal structure are based on the results of X-ray diffraction (XRD, Bruker D8 type) in the range of 5–90°, which was measured by Bruker D8 type (filtered Cu Kα radiation, $\lambda = 1.5418$ Å). Raman spectroscopy (Horiba Jobin-Yvon, LabRAM HR800c) was selected to evaluate defects in spent graphite and F-RG. The X-ray photoelectron spectroscopy (XPS) surface analysis in this work is performed by the Thermofisher Escalab Xi+ (Al Kα). Fourier transform infrared spectroscopy (FTIR, PerkinElmer Spectrum 100) was used to collect the spectra of the flash products. Inductive Coupled Plasma Emission Spectrometer (ICP, Thermo ICAP-7400) was used to detect metal element residues in spent graphite and F-RG. Thermogravimetric

analysis (TG) was performed to check the removal degree of the impurities using the NETZSCH STA 449F5 thermogravimetric analyzer under a nitrogen atmosphere.

4.3 | Electrochemical measurements

The anode slurry was prepared by mixed 80 wt% F-RG, 10 wt% Super-P, and 10 wt% carboxymethylcellulose (CMC) evenly through magnetic stirring. The slurry was poured onto the copper foil and scraped to a thickness of 300 μm. Then the copper foil coated with the slurry at a thickness of 300 μm was vacuum dried under 120°C and cut to the appropriate size. The electrode with the mass loading of F-RG or spent graphite around 2 mg cm^{-2} were selected, while the lithium metal were used as a reference electrode to assemble the CR2032 coin-type half-cells in an argon glove box. Two electrodes were separated by a Celgard 2400 membrane. Using 1 M $LiPF_6$ solution in equal-volume-mixing EC-DMC-EMC as the electrolyte.

For the full-cell assembly, the copper foil was cut into a rectangle and assembled with the new commercial $LiFePO_4$ cathode into a stacked battery, which was thermally packaged by aluminum plastic. Each active substance has a load of about 100 mg, and the electrolyte injection amount is 1 g.

The electrochemical performances of assembled batteries including cyclic voltammetry curves (CV) and electrochemical impedance spectroscopy (EIS, 100 kHz–0.01 Hz) were measured on a multichannel electrochemical analyzer produced by Ivium Technologies. The half and full cells were applied the galvanostatic charge–discharge (GCD) at different current densities and cycle GCD on a battery test system (NEWARE BTS-5V20mA, NEWARE Technology Co., Ltd.). The voltage windows relates to the calculations of specific capacity, capacity retention, and lithium-ion diffusion coefficient were 0.01–3 V (half-cell) and 1–4.2 V (full cell).

ACKNOWLEDGMENTS

This work was supported by the National Natural Science Foundation of China (51702063, 51672056), Natural Science Foundation of Heilongjiang (LC2018004), China Postdoctoral Science Foundation (2018M630340, 2019T120254), and the Fundamental Research Funds for the Central University.

CONFLICT OF INTEREST

The authors declare no conflict of interest.

ORCID

Jun Yan https://orcid.org/0000-0002-9967-3912
Kai Zhu https://orcid.org/0000-0002-9451-0890

REFERENCES

1. Goodenough JB. Electrochemical energy storage in a sustainable modern society. *Energy Environ Sci*. 2014;7(1):14-18.
2. Gür TM. Review of electrical energy storage technologies, materials, and systems: challenges and prospects for large-scale grid storage. *Energy Environ Sci*. 2018;11(10):2696-2767.
3. International Energy Agency, Total Installed Battery Storage Capacity in The Net Zero Scenario, 2015-2030. Accessed February 2, 2022. https://www.iea.org/reports/energy-storage.
4. Fan E, Li L, Wang Z, et al. Sustainable recycling technology for Li-ion batteries and beyond: challenges and future prospects. *Chem Rev*. 2020;120(14):7020-7063.
5. Xiang J, Yang L, Yuan L, et al. Alkali-metal anodes: from lab to market. *Joule*. 2019;3(10):2334-2363.
6. Andersen HL, Djuandhi L, Mittal U, Sharma N. Strategies for the analysis of graphite electrode function. *Adv Energy Mater*. 2021;11(48):2102693.
7. Cheng XB, Zhang R, Zhao CZ. A perspective on sustainable energy materials for lithium batteries. *SusMat*. 2021;1(1):38-50.
8. Cai WL, Yan C, Yao YX, et al. Rapid lithium diffusion in order@disorder pathways for fast-charging graphite anodes. *Small Struct*. 2020;1(1):2070001.
9. Natarajan S, Aravindan V. An urgent call to spent lib recycling: whys and wherefores for graphite recovery. *Adv Energy Mater*. 2020;10(37):2002238.
10. Jaberwock Research, Who Will Supply Graphite to The Fast-Growing Battery Industry? Accessed February 2, 2022. https://seekingalpha.com/article/3985951.
11. Tan DHS, Chen YT, Yang H, et al. Carbon-free high-loading silicon anodes enabled by sulfide solid electrolytes. *Science*. 2021;37(6562):1494-1499.
12. Jiang LL, Yan C, Yao YX, Cai W, Huang JQ, Zhang Q. Inhibiting solvent co-intercalation in a graphite anode by a localized high-concentration electrolyte in fast-charging batteries. *Angew Chem Int Ed*. 2021;60(7):3402-3406.
13. Luong DX, Bets KV, Algozeeb WA, et al. Gram-scale bottom-up flash graphene synthesis. *Nature*. 2020;577(7792):647-651.
14. Chen W, Li JT, Wang Z, et al. Ultrafast and controllable phase evolution by flash joule heating. *ACS Nano*. 2021;15(7):11158-11167.
15. Stanford MG, Bets KV, Luong DX, et al. Flash graphene morphologies. *ACS Nano*. 2020;14(10):13691-13699.
16. Advincula PA, Luong DX, Chen W, Raghuraman S, Shahsavari R, Tour JM. Flash graphene from rubber waste. *Carbon*. 2021;178:649-656.
17. National Insitute of Standards and Technology, NIST Chemistry WebBook, 10.18434/T4D303,.
18. Zhang H, Yang Y, Ren DS, Wang L, He XM. Graphite as anode materials: fundamental mechanism, recent progress, and advances. *Energy Storage Mater*. 2021;36:147-170.
19. Liang HJ, Hou BH, Li WH, et al. Staging Na/K-ion de-/intercalation of graphite retrieved from spent Li-ion batteries: in operando x-ray diffraction studies and an advanced anode material for Na/K-ion batteries. *Energy Environ Sci*. 2019;12(12):3575-3584.
20. Dong S, Song YL, Fang YZ, et al. Microwave-assisted synthesis of carbon dots modified graphene for full carbon-based potassium ion capacitors. *Carbon*. 2021;178:1-9.
21. Ferrari AC, Basko DM. Raman spectroscopy as a versatile tool for studying the properties of graphene. *Nat Nanotechnol*. 2013;8(4):235-246.

22. Nie M, Chalasani D, Abraham DP, Chen Y, Bose A, Lucht BL. Lithium ion battery graphite solid electrolyte interphase revealed by microscopy and spectroscopy. *J Phys Chem C*. 2013;11(3):1257-1267.
23. Zhao YM, Ren LX, Wang AX, et al. Composite anodes for lithium metal batteries. *Acta Phys -Chim Sin*. 2021;37:2008090.
24. Tripathi AM, Su WN, Hwang BJ. In situ analytical techniques for battery Interface analysis. *Chem Soc Rev*. 2018;47(3):736-851.
25. Tucureanu V, Matei A, Avram AM. FTIR spectroscopy for carbon family study. *Crit Rev Anal Chem*. 2016;46(6):502-520.
26. Liu D, Shadike Z, Lin R, et al. Review of recent development of in situ/operando characterization techniques for lithium battery research. *Adv Mater*. 2019;31(28):e1806620.
27. Liu TC, Lin LP, Bi XX, et al. In situ quantification of Interphasial chemistry in Li-ion battery. *Nat Nanotechnol*. 2019;14(1):50-56.
28. Barai A, Uddin K, Dubarry M, et al. Comparison of methodologies for the non-invasive characterisation of commercial Li-ion cells. *Prog Energy Combust Sci*. 2019;72:1-31.
29. Mason Graphite Inc., Typical Applications for Value-Added Products. Accessed February 2, 2022. https://masongraphite.com/value-added-project/.
30. Moradi B, Botte GG. Recycling of graphite anodes for the next generation of lithium ion batteries. *J Appl Electrochem*. 2015;46(2):123-148.
31. Ye L, Wang CH, Cao L, et al. Effective regeneration of high-performance anode material recycled from the whole electrodes in spent lithium-ion batteries via a simplified approach. *Green Energy Environ*. 2021;6(5):725-733.
32. Rothermel S, Evertz M, Kasnatscheew J, et al. Graphite recycling from spent lithium-ion batteries. *ChemSusChem*. 2016;9(24):3473-3484.
33. Da HR, Gan M, Jiang DF, Xing CX, et al. Epitaxial regeneration of spent graphite anode material by an eco-friendly in-depth purification route. *ACS Sustain Chem Eng*. 2021;9(48):16192-16202.
34. Markey B, Zhang H, Robb I, et al. Effective upcycling of graphite anode: healing and doping enabled direct regeneration. *J Electrochem Soc*. 2020;167(16):160511.
35. Cao N, Zhang YL, Chen L, et al. An innovative approach to recover anode from spent lithium-ion battery. *J Power Sources*. 2021;483:229163.
36. Gao Y, Wang CY, Zhang JL, et al. Graphite recycling from the spent lithium-ion batteries by sulfuric acid curing-leaching combined with high-temperature calcination. *ACS Sustain Chem Eng*. 2020;8(25):9447-9455.
37. Gao Y, Zhang JL, Jin H, et al. Regenerating spent graphite from scrapped lithium-ion battery by high-temperature treatment. *Carbon*. 2022;189:493-502.
38. Zhang JK, Lei Y, Lin ZP, Xie P, Lu H, Xu J. A novel approach to recovery of lithium element and production of holey graphene based on the lithiated graphite of spent lithium ion batteries. *Chem Eng J*. 2022;436:135011.
39. Beckham JL, Wyss KM, Xie YC, et al. Machine learning guided synthesis of flash graphene. *Adv Mater*. 2022;34(12):2106506.

SUPPORTING INFORMATION

Additional supporting information may be found in the online version of the article at the publisher's website.

How to cite this article: Dong S, Song Y, Ye K, et al. Ultra-fast, low-cost, and green regeneration of graphite anode using flash joule heating method. *EcoMat*. 2022;4(5):e12212. doi:10.1002/eom2.12212